A&A 438, 663–673 (2005)
DOI: 10.1051/0004-6361:20052722

Astronomy & Astrophysics

L-band (3.5 μm) IR-excess in massive star formation

I. 30 Doradus⋆

M. Maercker[1,2] and M. G. Burton[2]

[1] Stockholm Observatory, AlbaNova University Center, 106 91 Stockholm, Sweden
e-mail: maercker@astro.su.se
[2] School of Physics, University of New South Wales, Sydney, NSW 2052, Australia
e-mail: mgb@phys.unsw.edu.au

Received 18 January 2005 / Accepted 18 April 2005

Abstract. *L*-band data of 30 Doradus at 3.5 μm taken with SPIREX (South Pole Infrared Explorer) is presented. The photometry was combined with 2MASS *JHK* data at 1.25−2.2 μm. Colour−colour and colour−magnitude diagrams are constructed and used to determine the sources with infrared excess. These are interpreted as circumstellar disks, and enable the fraction of sources with disks (the cluster disk fraction or CDF) to be determined. We find that ∼42% of the sources detected at *L*-band in 30 Doradus have an IR-excess.

Key words. stars: circumstellar matter – stars: formation – stars: evolution – Hertzsprung-Russell (HR) and C-M diagrams – planetary systems: protoplanetary disks – stars: pre-main sequence

1. Introduction

1.1. IR-excess as a measure of circumstellar disks

During star formation, young stellar objects (YSOs) are associated with the circumstellar material surrounding them, making them bright at infrared wavelengths as the dust absorbs and re-emits radiation from the central star. As the star evolves towards the main sequence, the distribution of the surrounding material also changes, as is evident through the changing spectral energy distribution (SED) of the source. SEDs can therefore be used as an indicator of the evolutionary state of a YSO. In particular, an excess in IR radiation above that of a blackbody for class II/III YSOs can be explained by models of circumstellar disks around protostars (e.g. Lada & Adams 1992). In IR colour−colour diagrams, such stars lie outside the region defined by the reddening band to the main sequence. Colour−colour diagrams can therefore be used to identify the stars with circumstellar disks in star forming regions, and to estimate what fraction of the population this represents.

1.2. L-band over K-band

The excess emission is measurable in the *K*-band at 2.2 μm, making infrared excess detectable using *JHK* (1−2.2 μm) observations. However, this radiation may be caused by a circumstellar disk, the protostellar envelope or emission nebulosity from HII regions and therefore *JHK* band observations alone may not be sufficient to determine the nature of the IR excess. *L*-band observations (3.5 μm) prove to be the ideal wavelength for detecting circumstellar disks (e.g. Kenyon & Hartmann 1995). Compared to *JHK* colour−colour diagrams, the stars with IR excess are much more clearly separated in *JHKL* colour−colour diagrams. Additionally, the continuum emission from the stellar photosphere is generally bright enough in *L*-band to allow the determination of the number of stars with IR excess compared to the total number of stars in a given region (i.e. the cluster disk fraction (CDF)). It is relatively easier to obtain *L*-band data with the same sensitivities and spatial resolution as *JHK* band observations than it is for mid-IR data, where the signature from disk emission is even more pronounced (e.g. Rathborne 2003).

1.3. 30 Doradus

30 Doradus in the Large Magellanic Cloud is the most luminous giant HII region in the Local Group of Galaxies (Kennicutt 1984) and is located at a distance of ∼55 kpc (Vermeij et al. 2002). Star formation within the region was first identified by Hyland et al. (1992). Walborn & Blades (1997) identify four phases comprising an age sequence for massive OB cluster evolution (Walborn 1991a,b) in five spatial and/or temporal structures. The region shows recent and ongoing star formation at discrete epochs, with a central cluster of massive

⋆ Full Table 6 is only available in electronic form at the CDS via anonymous ftp to cdsarc.u-strasbg.fr (130.79.128.5) or via http://cdsweb.u-strasbg.fr/cgi-bin/qcat?J/A+A/438/663

stars surrounded by extended nebulosity. The stellar population consists of multiple generations, with pre-main sequence stars, early type main sequence stars and evolved blue and red supergiants (Walborn & Blades 1997). Ages range from young stars less than 1 Myr old, to the giant population with ages up to 25 Myr. Two supernova remnant (SNR) candidates have also been identified (Lazendic et al. 2003). Using deep broadband *I* and *V* WFPC2 images from the HST, Sirianni et al. (2000) derived the IMF for the central cluster R136 in 30 Doradus down to 1.35 $M_{\odot}$, suggesting there are relatively fewer lower-mass stars than in the Galactic IMF (though this may also arise from not fully correcting for extinction from the source). IR and radio observations show molecular gas and warm dust concentrated in an arc to the north and west of the central cluster (Rubio et al. 1998). They found 84 IR sources linked with the nebular microstructures and early O stars in dense nebular knots. 6 of these could be matched with sources found in this paper (Table 6). Identification of early O-type stars was taken as evidence for star formation (Walborn & Blades 1997). These knots have been revealed to be compact multiple systems which are each similar to star forming regions in the Galaxy such as the Trapezium system in the Orion cluster (Brandner et al. 2001). In their paper Brandner et al. use near-IR colour−colour diagrams obtained from NICMOS data to identify pre-main sequence stars by their intrinsic IR-excess. It is suggested that the spatial distribution of these stars indicate the birth of an OB association. Present day star formation coincides with the dense regions of molecular gas (Johansson et al. 1998) to the north and west of R136 and with their interfaces with the cavity created by the central cluster (Brandner et al. 2001). It is the nearest and therefore most highly resolved starburst region outside the Galaxy, thus making it a suitable source to study extragalactic star formation.

This paper presents *L*-band photometry of the 30 Doradus region taken with the SPIREX telescope at the South-Pole. IR-excess is detected by combining the *L*-band data with *JHK*-data from 2MASS. Colour−colour and colour–magnitude diagrams are presented, with a discussion on the implications for massive star formation and the evolution of circumstellar disks. Section 2 describes the observational data. Section 3 presents the results of the photometry on the *L*-band images. Section 4 analyses the results and Sect. 5 provides an interpretation.

2. Observations

2.1. L-band data from SPIREX

The *L*-band data was taken using the 60 cm South Pole InfraRed Explorer (SPIREX) (Hereld 1994; Burton et al. 2000) at the Amundsen-Scott South-Pole station in the Antarctica in 1998 by the winter-over scientist Charlie Kaminsky. The telescope was equipped with an Aladdin 1024× 1024 InSb Abu detector with filters sensitive in the range from 2.4−5 μm. The camera provided a 10′ field of view with a pixel size of 0.6″. The diffraction limit of 1.4″, combined with seeing and tracking error, over the unguided observations, resulted in a typical resolution of 2.6″. Observations were taken through the *L*-band filter ($\lambda_{\rm central}$ = 3.514 μm, $\Delta\lambda$ = 0.618 μm) by taking one set of sky frames followed by two sets of object frames and another set of sky frames. Each set consisted of five averaged frames offset by approximately 30″ from the previous frame. This allowed for the easy removal of image artefacts from the array and sky emission and of stars in the sky frames. The total on-source integration time was 9.25 h. Reductions were done automatically by the RIT SPIREX/Abu pipeline[1]. This image was archival data from SPIREX, but unfortunately had not been flux-calibrated, requiring us to determine the calibration through seperate observations (see Sect. 2.3).

2.2. JHK-band data from 2MASS

The observations from SPIREX were complemented with the 2MASS point source catalogue (PSC) (Cutri et al. 2003) and Atlas Images[2]. The 2MASS telescopes scanned the sky in both hemispheres in three near infrared filters (*J*, *H* and *K*; 1.25, 1.65 and 2.2 μm respectively) and detected point sources in each band which were brighter than about 1 mJy using a pixel size of 2.0″. Two 1.3 m telescopes were used, located at Mt Hopkins in Arizona and CTIO in Chile. Each used a camera capable of observing in the bands simultaneously with the 256 × 256 arrays of HgCdTe detectors. The imaging was done while the highly automated telescopes scanned over the sky in declination at a rate of ∼1′ per second. The images consist of six pointings on the sky with a total integration time of 7.8 s (Kleinmann et al. 1994). The Atlas Images from the 2MASS catalogue were used to derive *K*-band magnitudes for sources seen in the *L*-band that could not be matched with the sources in the PSC.

2.3. Calibration data from CASPIR

In order to calibrate the SPIREX image, observations were carried out in early April 2004 using the Australian National University (ANU) 2.3 m telescope at Siding Spring Observatory, equipped with CASPIR (Cryogenic Array Spectrometer/Imager) (McGregor 1994). CASPIR is a cryogenic re-imaging camera with pixel scales of 0.5″/pixel and 0.25″/pixel and 2 different readout methods. The detector is a hybrid device with 256 × 256 pixels, capable of direct imaging and spectroscopy between 1−5 μm. To avoid saturation from the sky in the *L*-band, a narrow band filter ($\lambda_{\rm central}$ = 3.592 μm, $\Delta\lambda$ = 0.078 μm) had to be used as well as the smaller pixel scale, resulting in a 60″ field of view. The standard star used is listed in Table 1. The stars in 30 Doradus that were used to calibrate the remaining stars in the *L*-band images are listed in Table 2. These are bright and isolated stars in the SPIREX image. Comparison of the relative photometry of the five stars observed both with CASPIR and SPIREX indicates that individual errors of ±0.1 to ±0.2 mag are made, and taking the weighted average this leads to a zero point error of 0.04 mag. This has been included in all subsequent error calulcation.

[1] http://pipe.cis.rit.edu

[2] Available at http://www.ipac.caltech.edu/applications/2MASS/IM/

Table 1. Standard star used to calibrate the CASPIR images.

name	RA (J2000)	Dec (J2000)	m_L
	(h m s)	(d m s)	mag
BS2015	05 44 46.5	−65 44 08.0	3.711

Table 2. Stars in 30 Doradus used for calibration. Bright, isolated stars were chosen from the SPIREX image and used to calibrate the remaining stars in the image. Their *L*-band magnitudes and errors were determined from the standard star.

id	RA (J2000)	Dec (J2000)	m_L
	(h m s)	(d m s)	mag
11	05 38 06.6	−69 03 45.0	9.3 ± 0.2
14	05 38 09.6	−69 06 21.2	8.7 ± 0.1
26	05 38 16.7	−69 04 14.2	8.3 ± 0.1
28	05 38 17.0	−69 04 00.8	8.7 ± 0.2
29	05 38 17.6	−69 04 12.0	9.6 ± 0.1

3. Results

3.1. Photometry

The SPIREX *L*-band image of 30 Doradus is shown in Fig. 1. Figure 2 shows an enlargement of the central region overlaid with contours showing the nebulosity. A coordinate frame was fit to the SPIREX images using the *koords* program in the *Karma* package[3] and the 2MASS atlas images for the reference frame. Photometry was undertaken using the *IRAF/daophot* package[4]. The resulting fluxes were calibrated using the stars measured with CASPIR, to determine the zero point correction. Error estimation was done using the *addstar* package by adding 220 artificial stars and running the same analysis as on the original image. This resulted in a 90% completeness limit of 13.5 mag in *L*-band. In order to include stars from the 2MASS images possibly missed by the automated detection process used to create the PSC, the same analysis was run on the 2MASS *K*-band images. This resulted in 7 additional matches for sources in the *L*-band image that were not matched with the PSC.

Matches between the SPIREX and 2MASS images were confirmed visually by overlaying and blinking the images. For 24 stars no match for the *L*-band stars could be found with the *JHK* data. Table 4 summarizes the statistics of the detections in the various bands. The results of the photometry including errors are given in Table 6. Table 4 also lists the statistics in the various bands for detections brighter than the 90% *L*-band completeness limit.

Figure 3 shows a *HKL* colour image of the central region, showing the bright features seen in the *L*-band, indicating regions of massive star formation.

[3] http://www.atnf.csiro.au/karma/

[4] http://iraf.noao.edu/

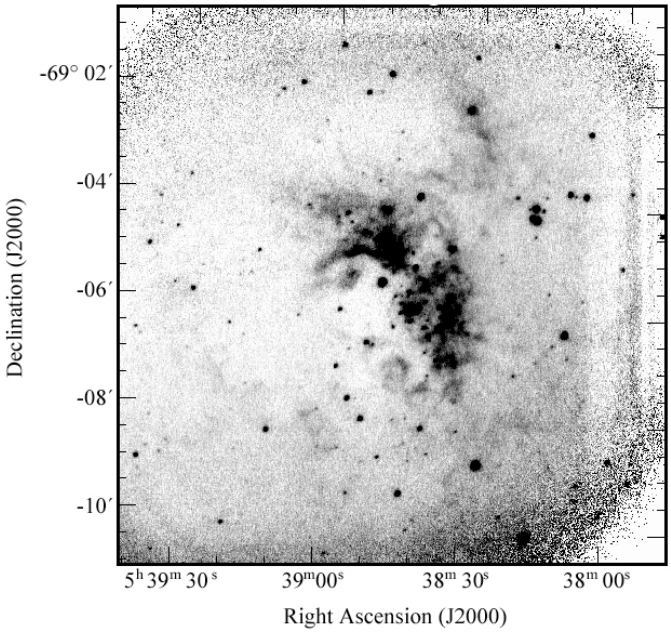

Fig. 1. SPIREX *L*-band (3.5 μm) image of 30 Doradus. Total integration time 9.25 h; effective resolution 2.6″; pixel scale 0.6″; 90% completeness limit at 13.5 mag; faintest star detected 14.5 mag.

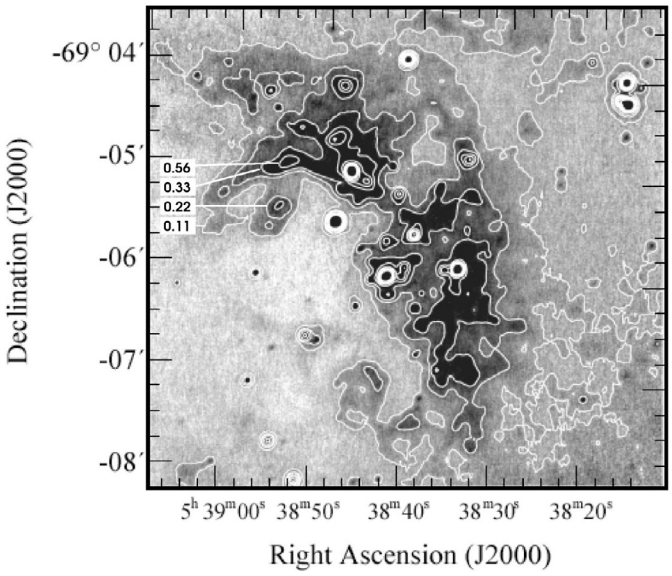

Fig. 2. Enlargements of the central region of 30 Doradus with contours showing the nebulosity. Contour levels are 0.11, 0.22, 0.33, 0.56, 0.75, 0.97, 1.19, 1.42 and 1.64 mJy/arcsec^2. The first four levels are labeled in the image. The image shows the nebulous arcs and denser knots in the central region. These denser regions coincide with the distribution of molecular gas (Johansson et al. 1998) and are believed to be regions of present day star formation.

3.2. Sensitivity

The detection threshold was assumed to be three times the background variation $\sigma_{\rm sky}$, the typical standard deviation of the background in a sky region near each source. This provides a limiting magnitude of $m_{\rm limit}$ = 13.5. This corresponds to the 90% completeness limit determined by adding artificial stars. However, the background is variable over the image,

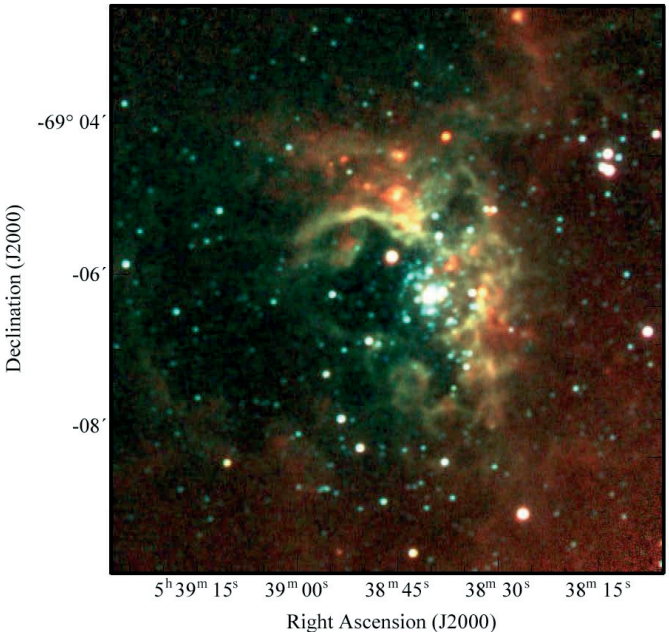

Fig. 3. *HKL* (Blue = *H*, Green = *K*, Red = *L*) composite colour image of 30 Doradus created using the 2MASS and SPIREX images. Regions bright in the *L*-band (3.5 μm) can be seen to the north-east and west of the central cluster, indicating the presence of young stellar objects.

particularly on account of nebulosity and source confusion in the more crowded regions. The faintest source detected has an *L*-band magnitude of 14.5, corresponding to a 78% completeness limit. This sensitivity has only recently been bettered by a ground-based telescope; Stolte et al. (2004) achieved a limiting magnitude of 15 at *L*-band using the 8 m VLT. This illustrates the improved sensitivity as a result of the low thermal background in Antarctica (100−300 mJy/arcsec^2 at 3.5 μm; Phillips et al. 1999).

3.3. Foreground contamination

Off-source comparison images were not available for the SPIREX images. An estimation of the foreground contamination therefore had to be made using the $(J-K)$ colours of the stars. If the visual extinction A_V to the source is known, the $(J-K)$ colour excess due to interstellar reddening between the Earth and the source can be calculated. Assuming that the majority of all source stars are embedded and therefore additionally reddened, any star bluer than this $(J-K)$ colour is likely to be a foreground star. Adopting an extinction parameter of $R_V = \frac{A_V}{E(B-V)}$ of ∼3.4 (Selman et al. 1999) and the $(B-V)$ and $(B-V)_0$ colours for sources in 30 Doradus (Walborn & Blades 1997) gives a visual extinction of ∼1.4 which corresponds to a limiting $(J-K)$ colour of ∼0.25.

An additional estimation of the $(J-K)$ colour of likely foreground stars was done using only the 2MASS data. 8 off-source fields with 3′ radii were extracted from the PSC and compared to a source field centred on 30 Doradus with a 7′ radius to encompass the entire area of the SPIREX image. The off-source fields were combined and the data was then plotted in *JHK* colour−colour diagrams and the number of IR-excess sources was determined. To minimise scatter in the colour−colour diagrams, only sources that lay above the sensitivity limit (*SNR* > 10) in each of the bands were included. The statistics for the field and source stars are listed in Table 3. As expected, the percentage of sources with an IR-excess is higher for source stars compared to field stars. Comparing these *JHK* colour−colour diagrams with similar diagrams for the entire LMC using 2MASS data (Nikolaev & Weinberg 2000) shows that these field stars occupy the same regions in the colour−colour diagrams with a similar scatter around the mean values, although the giant branch stretches much further along the reddening vector in the diagrams for the entire LMC data set.

Table 3. Statistics for the data from the 2MASS PSC for the combined off-source fields and the source field. The data for the field stars consists of 8 off-source fields with a 3′ radius each. The source data is a field centred on 30 Doradus with a radius of 7′. Only stars brighter than the sensitivity limit (*SNR* > 10) in all 3 bands (15.8, 15.1 and 14.3 for *J*, *H* and *K* respectively) were included.

Data	Number of stars per arcmin^2	Number of IR-excess sources per arcmin^2	Fraction (in %)
field	3.03	0.17	6
source	4.43	1.16	26

Table 4. Number of detections in the different bands. The first column gives the total number of detections in the SPIREX image. The second column gives the number of stars that could be matched with the 2MASS PSC. Column three lists the number of stars additionally matched by comparison of the *K*- and *L*-band images. The last column lists the number of stars only found in the SPIREX *L*-band image. The second row lists the respective numbers for stars brighter than the 90% completeness limit. Using the $(J-K)$ colour limit determined in Sect. 3.3 suggests 27 of the stars detected at *JHKL* are likely foreground stars.

	Total	*JHKL*	*KL*	*L*
All stars	215	184	7	24
$m_L < 13.5$ (90% limit)	199	171	4	24

As part of a comparison between the 2MASS data set and the Sloan Digital Sky Survey, Finlator et al. (2000) trace stellar spectral sequences in *JHK* colour−colour diagrams derived from the 2MASS data. These show that stars of type M5 and later lie at $(H-K_S) \sim 0.2$ and $(J-H) \sim 0.6$. The sequence moves to bluer $(H-K_S)$ and $(J-H)$ colours for stars of type G5 and earlier, with $(H-K_S) \sim 0.05$ and $(J-H) \sim 0.3$ giving a $(J-K)$ colour of ∼0.35. The distribution of $(J-K)$ colours over the source (Fig. 4) using the 2MASS data indeed shows a peak at $(J-K) \sim 0.35$ with an additional peak at $(J-K) \sim 1$ and a low rise in sources with even redder $(J-K)$ colours at $(J-K) \sim 2.4$. Both peaks can be found again in the same diagram for the field stars (Fig. 5), although here the peak at $(J-K) \sim 1$ is higher and the very red sources are missing. The $(J-K)$ distribution for the sources with complete *JHKL* data (Fig. 6) follows the same distribution as in Fig. 4

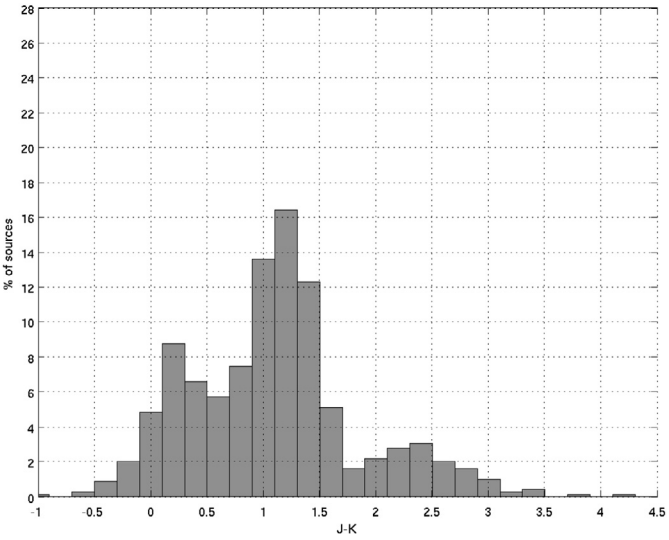

Fig. 4. $(J - K)$ colour distribution of *JHK* 2MASS data over the source. There is a peak at $(J - K) \sim 0.35$ which corresponds to the mean colour of stars earlier than G5 in the 2MASS PSC (Finlator et al. 2000). Another large peak occurs at $(J - K) \sim 1$. Redder sources with $(J - K) > 1.75$ are also present. The median error in $(J - K)$ is $\sigma_{(J-K)} = 0.08$.

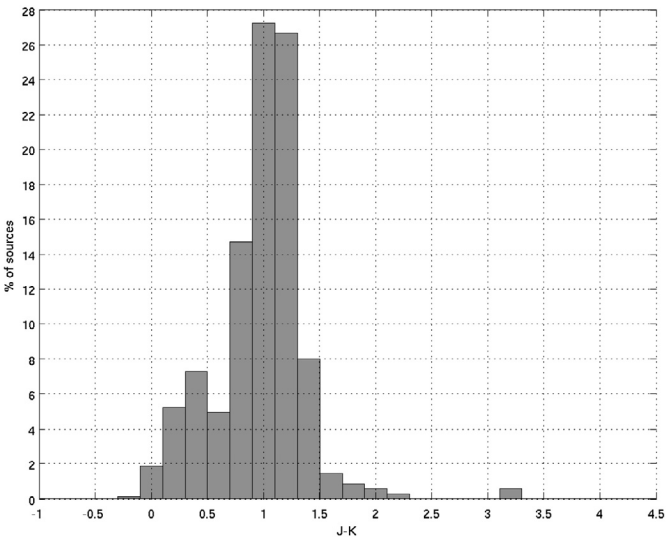

Fig. 5. $(J - K)$ colour distribution of the *JHK* 2MASS data for the field stars. The peak at $(J - K) \sim 0.35$ is still present, but is not as clear as in Fig. 4. The peak at $(J - K) \sim 1$ is higher and red sources with $(J - K) > 1.4$ are essentially missing. The median error in $(J - K)$ is $\sigma_{(J-K)} = 0.06$.

for the 2MASS data, indicating that $(J - K)$ colour limits determined using the 2MASS *JHK* data are also applicable to the *JHKL* data. Assuming that the bulk of the stars in the off-source fields are foreground (i.e. not part of the 30 Doradus complex), sources bluer than the $(J - K) = 0.35$ colour limit are therefore likely to be foreground. 27 such sources are found, as indicated in Table 6. 12 of these have a moderate IR-excess ($(K - L) \lesssim 0.6$) and three a slightly larger value (of $(K - L) = 1.1$, 1.3 and 2.5 respectively). Excluding these stars decreases the

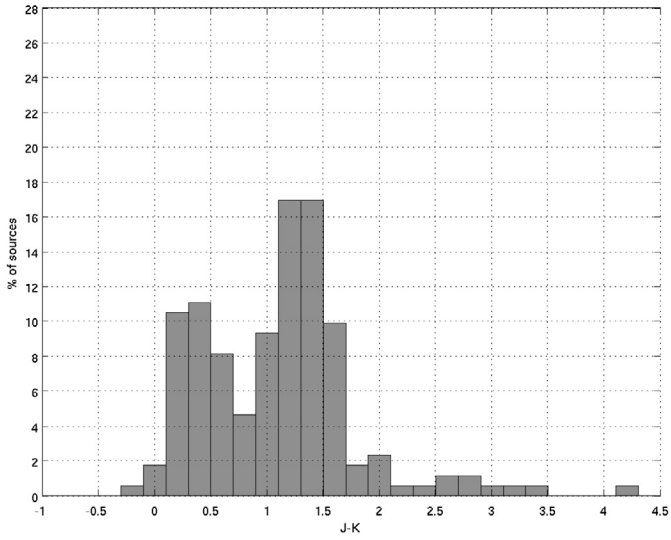

Fig. 6. $(J - K)$ distribution of the sources detected in all *JHKL* bands in 30 Doradus. This distribution is similar to the distribution in Fig. 4, with both peaks at $(J - K) \sim 0.35$ and $(J - K) \sim 1$ and red sources, indicating that the limits derived using the 2MASS *JHK* data also apply to the *JHKL* data. The median error in $(J - K)$ is $\sigma_{(J-K)} = 0.05$.

cluster disk fraction from 43% to 42% (see Sect. 5.1) (Table 5). Likely foreground stars are marked with boxes in Figs. 7 to 9.

4. Analysis

4.1. Colour–colour and colour–magnitude diagrams

Colour−colour and colour–magnitude diagrams were created using the 2MASS *JHK*-band and the SPIREX *L*-band magnitudes. Only sources that were brighter than the 90% completeness limit in *L*-band were used in creating the diagrams and determining the fraction of IR-excess sources. Using the intrinsic $(V - K)$, $(J - K)$, $(H - K)$ and $(K - L)$ colours of the main sequence and giant stars (Koornneef 1983) and their absolute visual magnitudes M_V (Allen 1973), the locations of the main sequence (spectral types O6-8 to M5) and the giant branch (spectral types K0 to M5) were plotted in all diagrams using a distance modulus of 18.7 mag.

Figures 7 to 9 show these colour−colour and colour−magnitude diagrams for 30 Doradus. In Figs. 7 and 8 the thick solid curve shows the main-sequence. In Fig. 9 the main sequence for stars ealier than type B0 is represented by the thick solid curve. In all diagrams the thin solid curve shows the giant branch for types between K0 and M5. The dashed curve shows the reddening vector up to $A_V = 30$ mag, assuming an extinction law $\propto \lambda^{-1.7}$.

4.2. Fraction of reddened sources

A large number of stars in the *JHKL* diagram lie well to the right of the reddening band, indicating an IR-excess. In determining the IR-excess the individual errors of all stars were used (Table 6). All stars which lie at least 1σ of their individual photometric error to the right and below the reddening band in the *JHKL* plane are defined to have an IR-excess and are

Table 5. Number of stars found with IR-excess and the reddening fraction. Numbers in the *JHKL*, *KL* and *L* columns are the number of stars with IR-excess found in the respective bands. These are listed assuming 1σ and 2σ distances from the reddening band. Columns 7 and 8 give the total number of sources with IR-excess at 1σ and 2σ. Column 9 gives the cluster disk fraction. Excluding possible foreground stars decreases the CDF to ∼42%. Only sources that are brighter than the 90% completeness limit (13.5 mag in *L*-band) are included when calculating the fraction of IR-excess sources.

JHKL (1σ)	*JHKL* (2σ)	*KL* (1σ)	*KL* (2σ)	*L* (1σ)	*L* (2σ)	total (1σ)	total (2σ)	frac
64	58	4	3	18	17	86	78	43 ± 5%

Table 6. (The complete table (215 rows) is only available in electronic form at the CDS). Magnitudes for all sources (including foreground sources and sources below the 90% completeness limit) in 30 Doradus. Stars with measurements in all four bands are listed first. Then stars with measurements in *K* and *L* only, and finally stars just detected in *L*-band. Column 1 gives the source id. Columns 2 and 3 the RA and Dec respectively in J2000. The coordinates for sources found in all four bands are from the point source catalogue, positions for the remaining stars are determined from reference 2MASS images. Columns 4, 6, 8 and 10 give the *JHK*- and *L*-band magnitudes respectively. Columns 5, 7, 9 and 11 give the photometric errors. For sources detected in all bands, the *JHK* magnitudes and errors are taken from the 2MASS PSC. A "null" as error indicates that no photometric error was given in the PSC. The *L*-band errors are combined from the errors in daophot and the errors due to the zero point correction. Sources only detected in the *K*- and *L*-bands have magnitudes from this work. For sources not detected at *J*, *H* or *K* the upper limits on these magnitudes are 15.8, 15.1 and 14.3 respectively. Stars with an IR-excess are marked with an "e" in Col. 12 (comments). Likely foreground stars are marked with "fg". Stars that matched sources in Rubio et al. (1998), Brandner et al. (2001) and Parker et al. (1993) are marked with "Rubio", "Brandner" and "Parker" respectively together with the id assigned in the respective papers.

id	RA (J2000) (h m s)	Dec (J2000) (d m s)	m_J	σ_J	m_H	σ_H	m_K	σ_K	m_L	σ_L	comments
1	5 37 50.2	−69 04 24.2	10.0	0.02	09.5	0.02	09.4	0.02	09.7	0.05	
2	5 37 50.5	−69 04 02.3	14.7	0.04	12.8	0.03	11.4	0.02	09.4	0.05	e
3	5 37 54.7	−69 09 03.2	10.3	0.02	09.4	0.02	09.1	0.02	09.1	0.08	
4	5 37 57.0	−69 03 38.9	12.9	0.02	11.9	0.03	11.6	0.03	10.8	0.05	e
5	5 37 58.1	−69 05 03.8	12.6	0.02	11.6	0.03	11.2	0.02	10.9	0.05	
⋮											

marked with the star symbol. To estimate the uncertainty in this number, the number of stars that lie a 2σ distance to the right and below the reddening vector was also calculated. This procedure excludes 6 stars from the *JHKL* data set, one star from sources found only in *K*- and *L*-band and also one star from those seen at *L*-band only. The variation of the number of stars to the right of the reddening band when assuming 1σ and 2σ distances is taken as an estimate of the uncertainty of the number of stars that have an IR-excess. Stars defined to have an IR-excess in the *JHKL* plane are marked with the same symbol in Figs. 8 and 9 as well. In the colour−magnitude diagram (Fig. 9) we can also include stars seen just at *K* and *L* (diamond shaped symbols). We also include those seen only in the *L*-band by providing a lower limit on the $(K - L)$ colour (circle symbols) since the 2MASS sensitivity limit at *K* is 14.3 mag. These stars therefore lie to the right of the circles in these diagrams. This makes it possible to also estimate what stars seen in just *K*- and *L*-bands have an IR-excess, by comparing their location in Fig. 9 to the stars already identified as having an IR-excess based on *JHKL* colours. Four of the stars seen only at *K* and *L* lie in the same region and are considered to have an IR-excess, and so are counted towards the total disk fraction. 18 of the stars seen just in *L*-band are also located in this region and are also counted towards the total disk fraction. Table 5 lists these statistics. Excluding stars bluer than $(J - K) = 0.35$, as discussed in Sect. 3.3, decreases the fraction of reddened stars in Table 5 by ∼1%.

4.3. Mass range

Figure 10 shows the number of detected sources vs. *L*-band magnitude for all sources in the SPIREX image. At the distance of 30 Doradus O3 main sequence stars have *L*-band magnitudes of 12.8, O6-8 main sequence stars have magnitudes of ∼13.9 and B0 main sequence stars have *L*-band magnitudes of ∼15.5. Masses can be crudely estimated by comparing the magnitudes with those for stars of known spectral type (Allen 1973). The histogram in Fig. 10 peaks at $m_L \sim 12$ mag, showing that we are mainly picking up the massive, early main sequence stars, extending down to masses of order 20 $M_\odot$ (i.e. late-type O stars). Figure 11 shows the percentage of stars in each magnitude interval that have an IR-excess. The distribution seems to peak closer to $m_L \sim 11$ mag, suggesting that the IR-excess possibly is not independent of mass. However, the IR-excess biases these estimates to higher mass. IR-excess is detected for masses down to ∼23 $M_\odot$, confirming that 30 Doradus is a region of high mass star formation.

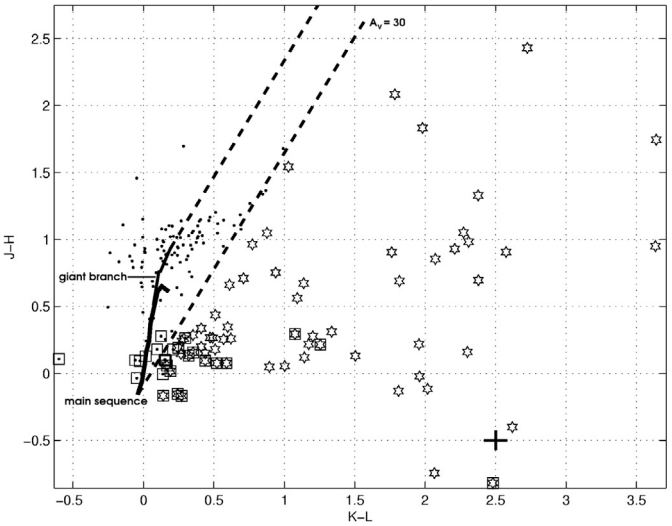

Fig. 7. *JHKL* colour−colour diagram for 30 Doradus. The thick solid line is the main sequence for spectral types O6-8 to M5. The thin solid line is the giant branch for spectral types K0 ($(J-H) = 0.5$, $(K-L) = 0.07$) to M5 ($(J-H) = 0.9$, $(K-L) = 0.19$), but is hard to see due to the number of stars in that region. Dashed lines are the reddening vectors up to $A_V = 30$. Star shaped symbols are sources identified as having an IR-excess. Sources in squares are likely to be foreground stars (Sect. 3.3). Mean errors are indicated by the cross in the lower right of the diagram. 64 of the 171 stars detected in the *JHKL* bands lie outside the reddening band and are therefore counted as having an IR-excess. These are interpreted as coming from circumstellar disks around the stars (Sect. 5.1).

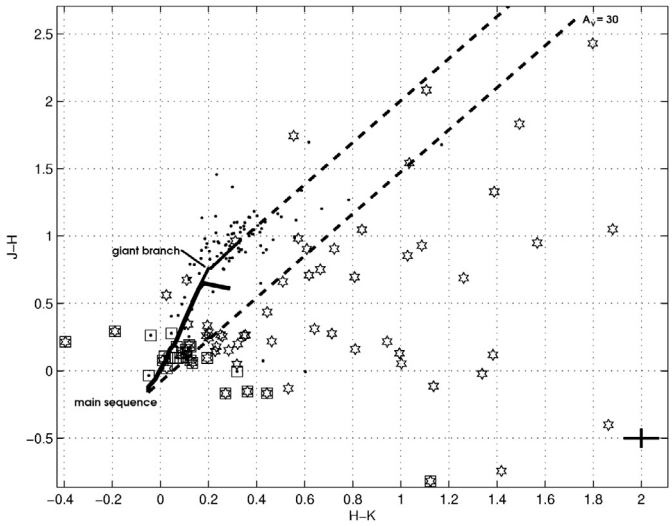

Fig. 8. *JHK* colour−colour diagram for 30 Doradus. The same symbols are used as in Fig. 7. Again the giant branch is hard to see, but extends from $(H-K) = 0.13$ to $(H-K) = 0.31$ with the same $(J-H)$ values as in Fig. 7. The diagram shows all sources detected in the *JHK*- and *L*-bands. The separation of stars with an IR-excess is much less clear in the *JHK* diagram than in the *JHKL* diagram. Based on the *JHK* data for these stars alone would only give 49 sources with IR-excess compared to 64 sources using the *JHKL* data (Table 5) leading to an understimate of the cluster disk fraction.

5. Discussion

5.1. IR-excess as an indicator of circumstellar disks

Using the *JHKL* data shows that $\sim 43 \pm 5\%$ of the stars detected in 30 Doradus at *L*-band lie to the right of the reddening band defined by interstellar extinction, and thus have an IR-excess over a stellar photosphere. Models for sources with circumstellar disks can explain such positions in the colour−colour diagrams (e.g. Lada & Adams 1992). Stars showing an IR-excess in the colour−colour and colour–magnitude diagrams (Table 5) are interpreted as having circumstellar disks. The cluster disk fraction (CDF) is therefore estimated as the fraction of stars with IR-excess.

5.2. Spatial distribution of IR-excess sources

Figure 12 shows the spatial distribution of the detected stars in the central part of the SPIREX image (see also Fig. 3). It is apparent that stars that do not show an IR-excess lie outside the nebulous regions, whereas IR-excess stars lie within the central nebula and along the arcs and knots in the image. Sources not detected in the *J*- and *H*-bands are essentially confined to the string of nebulous regions in the centre. There seems to be a string of stars only detected in the *L*-band along the arc north of the central cavity. The centre of 30 Doradus itself lies in a halo of molecular gas (Garay et al. 1993) and the sources only found in *L*-band are found to preferentially lie in the regions where [CII] and CO line emission is detected

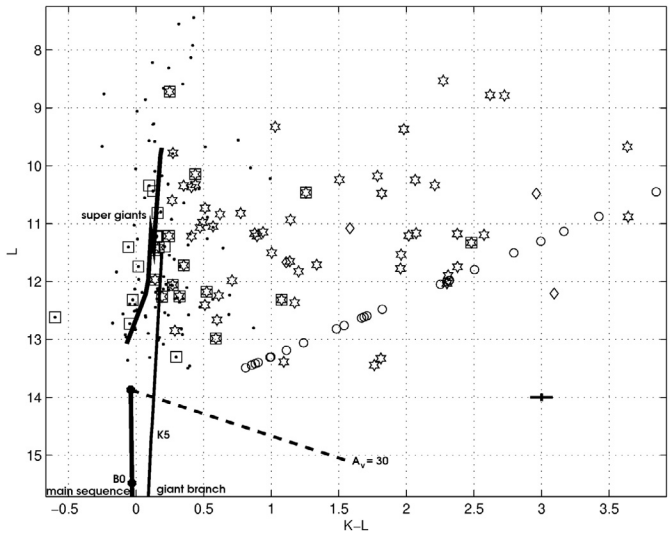

Fig. 9. Infrared *L* vs. $(K-L)$ colour–magnitude diagram for 30 Doradus. The lower thick solid line is the unreddened main sequence, the upper thick solid line shows the location of supergiants for a distance modulus of 18.7 mag. The dashed line shows reddening up to $A_V = 30$ mag. Star shaped symbols are sources with an IR-excess as determined from the *JHKL* diagram. Diamond symbols are stars only found in *K*- and *L*-bands. Circle symbols are stars only found in the *L*-band and are located at the lower limit for their $(K-L)$ colour. Sources in squares are likely to be foreground stars (Sect. 3.3). The position of the stars only found in the *KL*-bands and *L*-band can be compared to the location of stars with an IR-excess (star shaped symbols). Those occupying the same region are also counted as having an IR-excess, giving an additional 4 sources with an IR-excess found in *K* and *L*-bands and an additional 18 sources with an IR-excess found only in the *L*-band (Table 5).

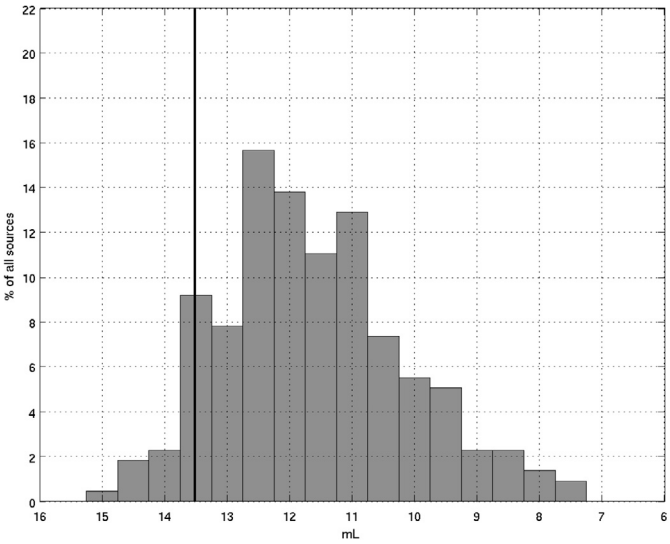

Fig. 10. *L* band luminosity function of all stars detected at *L*-band in the SPIREX image of 30 Doradus. Unreddened O3 main sequence stars have *L*-band magnitudes of 12.8 at the distance of 30 Doradus, unreddened O6-8 main sequence stars have magnitudes of ∼13.9 and unreddened B0 stars have *L*-band magnitudes of ∼15.5. The majority of detected stars have *L*-band magnitudes between 11 and 13, placing them where the massive, early type main sequence stars are. The vertical line at $m_L = 13.5$ shows the 90% completeness limit.

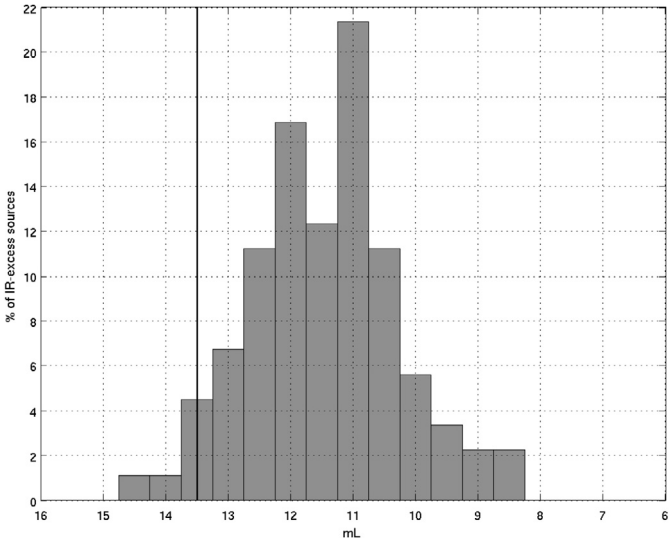

Fig. 11. The percentage of sources with an IR-excess in the different magnitude intervals. The distribution peaks at an *L*-band magnitude of ∼11 indicating high mass stars. IR-excess is however detected down to magnitudes of $L \sim 14.5$. The vertical line at $m_L = 13.5$ shows the 90% completeness limit.

(Poglitsch et al. 1995). IR-excess sources detected in all four bands tend to spread out further throughout the region.

5.3. Disk evolution

Together with the CDF and the age of the cluster, it is possible to estimate the lifetime of circumstellar disks. Walborn & Blades (1997) find several regions with different ages in

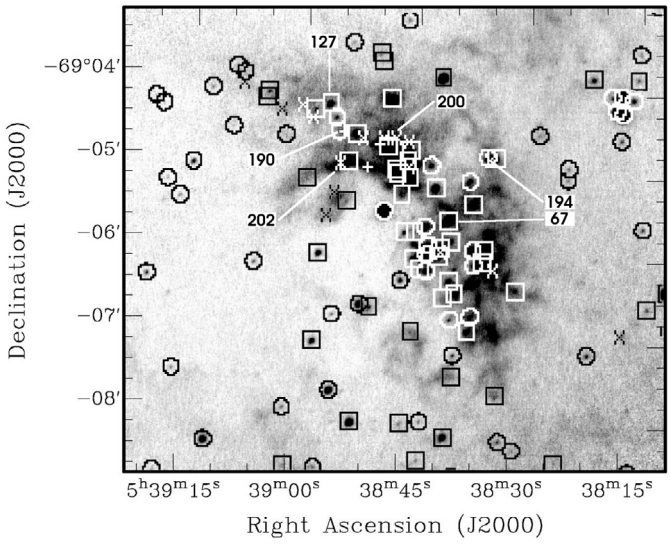

Fig. 12. Spatial distribution of sources in 30 Doradus. Circles mark stars without an IR-excess, squares mark stars with an IR-excess found in the *JHKL*-bands, plus signs mark stars with an IR-excess found only in the *KL*-bands and crosses mark stars with an IR-excess only found in *L*-band (there is no difference between white/black sources, this is only in order to make the stars in the nebulous regions more visible). A string of stars only detected in the *L*-band follows the nebulosity to the north-east of the central region. Stars with an IR-excess are confined to the inner regions inside the nebula. Sources without an IR-excess are mainly distributed in regions without any nebulosity. The 6 reddest stars ($(K - L) > 3$) are marked in the image with their id from Table 6.

the 30 Doradus region. The massive central region is estimated to be ∼2−3 Myr old, but a much younger population of less than 1 Myr and an older population of about 4−6 Myr are also found (Walborn & Blades 1997; Massey & Hunter 1998). Since young stars are very bright in the IR, sources with an IR-excess can be intepreted as being young stellar objects with some of these sources possibly being more deeply embedded protostars surrounded by dust shells rather than disks (Sect. 5.4). However, depending on the distribution of dust around evolved stars, these also present an explanation for the observed IR-excess and it would be necessary to take spectra of the sources to ascertain their evolutionary state.

Adopting a mean age for 30 Doradus of 2−3 Myr, the number of stars with IR-excess (∼42%; Table 5 excluding foreground stars) would imply that more than 50% of the circumstellar disks have disappeared after 2−3 Myr. It is possible that the intense radiation from the early type stars in the 30 Doradus region effectively destroys circumstellar disks and therefore decreases the CDF. Observations of HII regions in the Galaxy have shown that externally illuminated circumstellar disks get photoevaporated and disappear after 0.01−0.1 Myr. This has for example been seen in the proplyds in the Orion Nebula (O'Dell & Wen 1994). Proplyds are disks or flattened envelopes of circumstellar material that are photoevaporated from the outside by an external ionizing field. The variation in the form of proplyds is explained by a balance between stellar gas pressure and radial pressure and radiation pressure from dominant stars in the region. If this is the case for 30 Doradus,

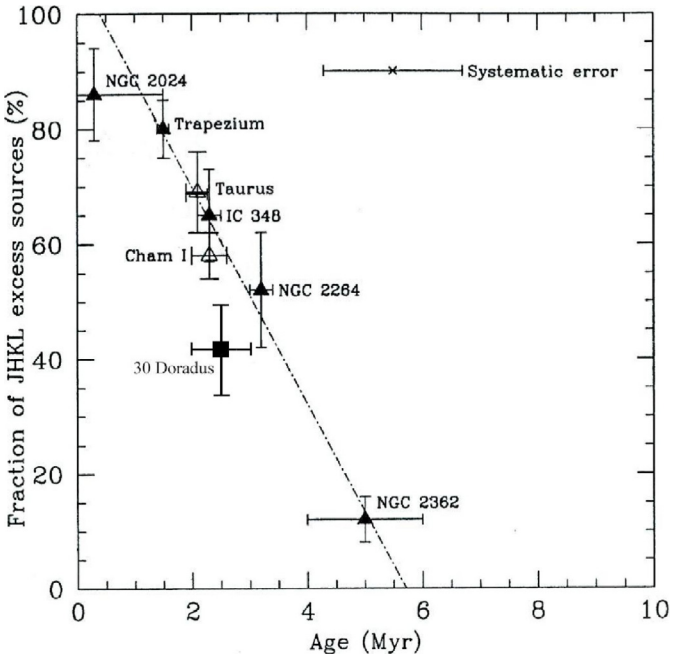

Fig. 13. Cluster disk fraction (CDF) for 6 clusters by Haisch et al. (2001b) vs. their mean ages. The CDFs were determined using *JHKL* data as described in their paper. The location of 30 Doradus is indicated by a square with error bars indicating the uncertainty in age and disk fraction. The dot-dashed line is the best fit determined by Haisch et al. (2001b).

the lifetime for disks estimated using the CDF of this region would be too low, and derived lifetimes a lower limit.

Combined with earlier *JHKL* observations (Haisch et al. 2001b) of clusters NGC 2264, NGC 2362, NGC 1960 (ages between 2.5−30 Myr) and younger clusters NGC 2024, Trapezium and IC 348, with ages down to 0.3 Myr (NGC 2024), predictions on the lifetime of circumstellar disks can be made. For all these clusters the fraction of sources with *JHKL* IR-excess is determined. Each cluster is then plotted in a CDF vs. age diagram (Fig. 13). The position of 30 Doradus in the diagram is indicated. The error in the CDF for 30 Doradus is ±8% due to the uncertainty in the number of IR-excess sources (±5%, Table 5) and allowing for an uncertainty in the number of foreground stars. The errors in the age reflect a mean age of 2−3 Myr. The location of 30 Doradus is consistent with the fit of Haisch et al., despite this being for sources which extend to much lower masses (0.13 $M_{\odot}$ for NGC 2024 up to 1 $M_{\odot}$ for NGC 2362 at the completeness limit; Haisch et al. 2001b) than our study of 30 Doradus.

A least-squares straight line fit to the data shows a linear relationship between disk fraction and cluster age. An estimated disk lifetime of 6 Myr is derived. The initial disk fraction appears to be very high ($\gtrsim$80%) and then declines linearly with increasing age. Taking the contamination of foreground stars into consideration yields a CDF of ∼42% and an age of ∼2.5 Myr, then the CDF derived here lies just below that which Haisch et al. would predict (Fig. 13). This indicates a quicker evolution of circumstellar disks around massive stars or that the disks indeed are being destroyed due to photoevaporation or possibly both.

5.4. High mass stars

Whereas 30 Doradus contains a large range of stellar masses (Brandner 2001), our observations are only sensitive to the most massive stars. Since the derived CDF lies at the lower end of the Haisch et al. prediction, this again indicates a faster evolution of circumstellar disks around massive stars. Previous studies of the 30 Doradus complex show 20 sources with IR-excess in *JHK* colour−colour diagrams (Brandner 2001). 8 of these could be matched with L-band sources found in the SPIREX image (Table 6) and have an IR-excess. The 20 sources were associated with Class I protostars and Herbig Ae/Be or T Tauri stars by comparing the measured colours with models. This again confirms the connection between star formation, circumstellar disks and IR-excess. The majority of sources in the Brandner paper however lie below the 2MASS detection limit (15.8 mag in J-band), which explains why we only identify 8 sources from their work. A scatter in the photometry of individual sources can be explained by differences in spatial resolution and nonstandard NICMOS passbands. In the Brandner study the sources of star formation were found to follow the densest regions of the molecular gas and the interface with the hollowed-out region from the central stars. The same is true for most of the 24 stars detected only in the L-band, which lie in the nebulous region north of the central star cluster (Fig. 12) (see Sect. 5.2). In the L vs. $(K - L)$ colour–magnitude diagram they occupy the same region as the IR-excess stars from the $(J - H)$ vs. $(K - L)$ colour−colour diagram. This makes it likely that these stars are in the process of forming and also contain circumstellar disks. These properties are characteristic of protostellar objects and the sources only detected in the L-band are possibly the equivalent of massive Class I protostars (Lada et al. 2000). Since these stars are only detected in the L-band, and not at shorter wavelengths, it also suggests they are heavily embedded in dust shells, and are massive young stellar objects.

5.5. The reddest sources

In Fig. 12 six particularly red sources ($(K - L) > 3$) are marked with their id from Table 6. Two of these are found in all four bands, one only in K and L and three are only found in L-band. The reddest source (#194, $(K - L) > 3.8$) lies in a knot to the north west of the central cluster. The other sources are in the central nebula and coincide with the brightest arcs and knots of the nebula. Three of the sources follow the chain of stars only detected in L-band towards the north-east of the image (#127, #190 and #200). Source #67 lies close to the central cluster.

5.6. Supergiants

The majority of the stars in the colour–magnitude diagram for 30 Doradus (Fig. 9) are located above the main sequence, meaning that these stars are brighter than O6-8 type stars (the sensitivity threshold of the SPIREX images lies at 13.5 mag, ∼0.4 mag brighter than the location of O6-8 stars). Massey & Hunter (1998) detected 31 O8V or earlier type stars in the 30 Doradus cluster. Other studies also find a significant number

of supergiants and giants (Walborn & Blades 1997; Bosch et al. 1999; Parker 1993). The location of supergiants between B0 and M0 is drawn in the 30 Doradus CMD in Fig. 9 as the upper thick solid line above the main sequence. Of the four papers on the stellar population quoted here, unfortunately, only Parker gives coordinates, so that it is not possible to match our data with the other three studies.

Matching a B0I supergiant and a O3V star from the Parker paper with the SPIREX data (stars #76 and #187, see Table 6) shows that these two stars indeed occupy the region of the CMD where most of the detected stars lie, making it likely that supergiant, giant and early type OV stars are present in 30 Doradus.

6. Conclusions

L-band photometry for 30 Doradus has been presented. Combining the *L*-band data with shorter wavelength data from the *JHK* bands proves to be a powerful method to detect IR-excess. In particular, this IR-excess can be interpreted as emission from circumstellar disks, making *L*-band observations an essential tool for identifying these disks. The clearer separation of stars in the *JHKL* diagrams provides a better estimate of the total cluster disk fraction than *JHK* data alone does. Only using *JHK* data tends to underestimate the number of stars with IR-excess (an analysis using the same stars as in the *JHKL* colour−colour diagram, but only considering the *JHK* information, gives only 49 IR-excess sources as compared to 64 when using the *JHKL* data (Table 5)). Comparing the results obtained for 30 Doradus with other *L*-band studies of star forming regions in the Galaxy shows an inverse relation between age and disk fraction, giving further support to an estimated disk lifetime of 6 Myr and a very high initial disk fraction. Since the sensitivity limit achieved for the observations in this study only includes stars of type O6 and brighter, these results indicate that high-mass stars form in a similar way to low-mass stars through circumstellar disks, however, it is possible that disks around high mass stars evolve faster than around low mass stars. Several sources are seen in the *L*-band image that are not found at shorter wavelengths. These sources are possibly heavily embedded, high-mass protostars. The positions of these stars in the colour–magnitude diagram indicate that they might also be circumstellar disk systems. It is also possible that the IR-excess originates from evolved stars (AGB stars) or young high and intermediate mass stars (see Sect. 5.3). In particular in the case of a complex environment with mutiple generations as 30 Doradus (see Sect. 1.3), a closer spectral examination is necessary to ascertain the evolutionary state of the sources.

No other extensive investigation of the *JHKL* colour excess has been made for 30 Doradus, making this the first study of infrared excess using *L*-band data for a significant number of stars for this region. The data are consistent with similar data obtained from Galactic sources, indicating that similar processes are at work in star formation in the LMC.

The data illustrates the ability of Antarctic telescopes, where the low thermal background improves IR sensitivity, to probe the state of the embedded stars in star forming regions.

Acknowledgements. This work could not have been conducted without the great help received from many colleagues within the US CARA and the Australian JACARA organisations whose efforts made the SPIREX/Abu project at the South Pole such a success, to whom we are extremely grateful. We also acknowledge the funding support from the Australian Research Council and the Australian Major National Research Facilities program that made this work possible in the first place. We thank the referee, Wolfgang Brandner, for his perceptive comments, which have greatly improved this paper. This publication makes use of data products from the Two Micron All Sky Survey, which is a joint project of the University of Massachusetts and the Infrared Processing and Analysis Center/California Institute of Technology, funded by the National Aeronautics and Space Administration and the National Science Foundation. This research has made use of the NASA/ IPAC Infrared Science Archive, which is operated by the Jet Propulsion Laboratory, California Institute of Technology, under contract with the National Aeronautics and Space Administration.

References

Allen, C. W. 1973, Astrophysical Quantities, 3rd ed., (London: The Athlone Press)
Bosch, G., Terlevich, R., Melnick, J., & Selman, F. 1999, A&AS, 137, 21
Brandner, W., Grebel, E. K., Barbá, R. H., Walborn, N. R., & Moneti, A. 2001, AJ, 122, 858
Burton, M. G., Ashley, M. C. B., Marks, R. D., et al. 2000, ApJ, 542, 359
Cutri, R. M., Skrutskie, M. F., van Dyk, S., et al. 2003, VizieR On-line Data Catalogue:II/246. Originally published in: University of Massachusetts and Infrared Processing and Analysis Center (IPAC/California Institute of Technology)
Finlator, K., Ivezic, Z., Fan, X., et al. 2000, AJ, 120, 2615
Garay, G., Rubio, M., Ramirez, S., Johansson, L. E. B., & Thaddeus, P. 1993, A&A, 274, 743
Haisch, K. E., Jr., Lada, E. A., & Lada, C. J. 2001a, AJ, 121, 2065
Haisch, K. E., Jr., Lada, E. A., & Lada, C. J. 2001b, ApJ, 553, L153
Hereld, M. 1994, ExA, 3, 87
Hyland, A. R., Straw, S., Jones, T. J., & Gatley, I. 1992, MNRAS, 257, 391
Johansson, L. E. B., Greve, A., Booth, R. S., et al. 1998, A&A, 331, 857
Kennicutt, R. C., Jr. 1984, ApJ, 287, 116
Kenyon, S. J., & Hartmann, L. 1995, ApJS, 101, 117
Kleinmann, S. G., Lysaght, M. G., Pughe, W. L., et al. 1994, Ap&SS, 217, 11
Koorneef, J. 1983, A&A, 128, 84
Lada, C. J., & Adams, F. C. 1992, ApJ, 393, 278
Lada, C. J., Muench, A. A., Haisch, K. E., Jr., et al. 2000, AJ, 120, 3162
Lazendic, J. S., Dickel, J. R., & Jones, P. A. 2003, ApJ, 596, 287
Massey, P., & Hunter, D. A. 1998, ApJ, 493, 180
McGregor, P., Hart, J., Downing, M., Hoadley, D., & Bloxham, G. 1994, ExA, 3, 139
Nikolaev, S., & Weinberg, M. D. 2000, ApJ, 542, 804

O'Dell, C. R., & Wen, Z. 1994, ApJ, 436, 194
Parker, J. W. 1993, AJ, 106, 560
Phillips, A., Burton, M. G., Ashley, M. C. B., et al. 1999, ApJ, 527, 1009
Poglitsch, A., Krabbe, A., Madden, S. C., et al. 1995, ApJ, 454, 293
Rathborne, J. 2003, Young Massive Stars: Traffic Lights for Nearby Star Formation, Ph.D. Thesis, University of New South Wales, Sydney
Rathborne, J., & Burton, M. G. 2005, in 25th IAU General Assembly, Sydney, July 2003, Highlights of Astronomy, ed. O. Engvold & M. Burton, ASP Conf. Ser., 13, in press
Rubio, M., Barbá, R. H., Walborn, N. R., et al. 1998, AJ, 116, 1708
Selman, F., Melnick, J., Bosch, G., & Terlevich, R. 1999, A&A, 341, 98
Sirianni, M., Nota, A., Leitherer, C., De Marchi, G., & Clampin, M. 2000, ApJ, 533, 203
Stolte, A., Brandner W., Brandl, B., Zinnecker, H., & Grebel, E. K. 2004, AJ, 128, 765
Vermeij, R., Peeters, E., Tielens, A. G. G. M., & van der Hulst, J. M. 2002, A&A, 382, 1042
Walborn, N. R. 1991a, The Magellanic Clouds, in Proceedings of the 148th Symposium of the International Astronomical Union, ed. R. Haynes, & D. Milne (Dordrecht: Kluwer Academic Publishers), 145
Walborn, N. R. 1991b, Massive Stars in Starbursts, in STScI Symp. 5, ed. C. Leitherer, N. R. Walborn, T. M. Heckman, & C. A. Norman (Cambridge: Cambridge Univ. Press)
Walborn, N. R., & Blades, J. C. 1997, ApJS, 112, 457